ISSN 2313-092X
E-ISSN 2411-9199
Ukrainian Black Sea Region Agrarian Science
Vol. 30, No. 2
UDC: 621.316.54:621.313:631.362
DOI: 10.56407/bs.agrarian/2.2026.76

The influence of dynamic operating modes of electric drives of pumping stations and grain drying complexes on the degradation of nanocomposite insulation of high-voltage circuit breakers: Measurement results and recommendations for agricultural engineering

Andrey Stavinskiy*
Doctor of Technical Sciences, Professor
Mykolaiv National Agrarian University
54008, 9 Georgiy Gongadze Str., Mykolaiv, Ukraine
https://orcid.org/0000-0001-7573-9238

Larisa Vakhonina
PhD in Physical and Mathematical Sciences, Associate Professor
Mykolaiv National Agrarian University
54008, 9 Georgiy Gongadze Str., Mykolaiv, Ukraine
https://orcid.org/0000-0002-1668-2275

Volodymyr Martynenko
PhD in Technical Sciences, Associate Professor
Mykolaiv National Agrarian University
54008, 9 Georgiy Gongadze Str., Mykolaiv, Ukraine
https://orcid.org/0000-0003-4067-3640

Vitalii Mardziavko
Master, Assistant
Mykolaiv National Agrarian University
54008, 9 Georgiy Gongadze Str., Mykolaiv, Ukraine
https://orcid.org/0000-0001-7327-9215

Andrii Rudenko
Master, Assistant
Mykolaiv National Agrarian University
54008, 9 Georgiy Gongadze Str., Mykolaiv, Ukraine
https://orcid.org/0000-0002-5103-6412

Abstract. The study was aimed at determining the impact of electrical, thermal and mechanical loads on the durability of polymer and nanocomposite insulation of high-voltage circuit breakers used in pumping stations and grain drying complexes in Ukraine. The methodology combined numerical modelling of electrostatic and thermal fields in three-dimensional structures of insulation units, accelerated thermal cycling and mechanical tests, partial discharge analysis according to international standards, thermographic control, microstructural studies and statistical assessment of resource based on reliability curves. It was found that traditional epoxy

Article's History:
Received: 22.12.2025 Revised: 20.04.2026 Accepted: 26.05.2026 Published: 30.06.2026

Suggested Citation:
Stavinskiy, A., Vakhonina, L., Martynenko, V., Mardziavko, V., & Rudenko, A. (2026). The influence of dynamic operating modes of electric drives of pumping stations and grain drying complexes on the degradation of nanocomposite insulation of high-voltage circuit breakers: Measurement results and recommendations for agricultural engineering. *Ukrainian Black Sea Region Agrarian Science*, 30(2), 76-95. doi: 10.56407/bs.agrarian/2.2026.76.

*Corresponding author (and-stavinskiy@outlook.com)

insulation undergoes the most intense degradation: after cyclic loads, the specific resistance decreased by 47.5%, the breakdown voltage by 25.7%, and the average service life was about 380 hours. For nano-filled material with silicon dioxide, the decrease in specific resistance was limited to 17%, breakdown voltage – 9.8%, with an increase in average resource to 715 hours. The highest stability was demonstrated by insulation with hexagonal boron nitride and internal shielding, for which changes in electrophysical parameters did not exceed 7.3% for specific resistance and 7.1% for breakdown voltage, the partial discharge onset voltage reached 5.5 kV, and the average resource was about 912 hours. Numerical and experimental results showed a decrease in the peak electric field strength from 8.6 to 5.4 kV/mm and maximum temperatures from 96.2 to 78.8°C after 1,000 start-up cycles. The use of controlled starting modes made it possible to reduce starting currents from 5.6 I_n to approximately 2.1 In and to reduce the integral thermal load on the insulation by 61.5%. A technical and economic assessment showed a reduction in the total cost of ownership over six months from USD 280 to USD 50 per insulation unit, confirming the practical feasibility of introducing nanocomposites and controlled starting modes in agro-industrial electric drives. The practical significance of the results obtained lies in the formation of criteria for the selection of materials and operating modes of electric drives in order to increase the reliability of switching equipment in agro-industrial electromechanical systems and the use of modelling and diagnostic approaches to predict degradation and optimise the design of insulation units

Keywords: partial discharges; epoxy resin; electrothermal load; dielectric strength; recoverable voltage; frequency regulation; microstructural defects

INTRODUCTION

In modern agro-industrial electrical systems, the reliability of high-voltage circuit breakers is determined by electromechanical load conditions, in which insulation components are subjected to starting currents, thermal fluctuations and vibrations. Such conditions create an environment in which polymer dielectrics demonstrate a decrease in resource stability, which necessitates the study of the complex influence of electrical, thermal, and mechanical factors on polymer and nanocomposite insulation. Within the framework of early diagnosis approaches, one of the methods under study is infrared thermography. In the work of M. Silnyk & V. Fedynets (2025), a correlation was established between temperature irregularities and areas of potential electrical instability, which determines the possibility of using this method to assess the technical condition of insulation components. The results obtained indicate that thermal anomalies correlate with areas of electrical defect formation, therefore thermographic monitoring can be used as a tool for early control of the insulation condition of circuit breakers.

This diagnostic paradigm is being expanded in the field of electrophysical processes: a study by A.A. Shcherba *et al*. (2023) found that the presence of non-sinusoidal voltages increases the activity of partial discharges (PD) in polymer dielectrics. The results obtained indicate a relationship between the nature of the voltage and the intensity of defect zone formation during repeated switching. In the field of insulation resource behaviour research, the work of O. Zidane *et al*. (2025) showed that repeated impulse overvoltages cause the accumulation of microdefects in the interturn insulation of electrical machines. The study noted that it is the pulsed nature of the voltage, rather than the prolonged action of nominal modes, that forms the main degradation patterns of the material. Similar trends were recorded in A. Stavinskiy *et al*. (2022), which analysed the unevenness of thermal fields in transformer nodes. The results showed that the design parameters of magnetic conductors determine the spatial distribution of temperature and affect the condition of adjacent dielectric elements.

In the mechanical dimension, M.V. Matvienko *et al*. (2023) investigated the role of interphase layers of lower stiffness, which create the conditions for stress concentration and microcrack formation under vibration loading. The authors demonstrated that repeated mechanical loads lead to progressive destruction precisely in the interphase regions. Mechanical and thermal effects also included the results of O.M. Kostin *et al*. (2022), which describe the uneven effect of thermal fields associated with arc processes on the surface layers of dielectric materials in switching devices. In the context of switching devices, these results explained the nature of defects that form during frequent starts of electric drives.

The understanding of the constructive impact on the condition of insulation systems has been expanded in the study by A. Stavinskii & D. Koshkin (2021), which showed that changing the configuration of steel transformer packages alters the distribution of heat flows in its nodes. It was found that local temperature increases

affect the rate of ageing of adjacent polymer elements, which is characteristic of equipment with long thermal cycles. Further development of this direction is presented in O.B. Iegorov *et al*. (2025), which analysed the impact of optimising the windings of synchronous reactive generators on electromagnetic and thermal processes. The work establishes that a change in design can reduce field unevenness and increase the stability of insulating materials in long-term operation. The starting modes of asynchronous electric drives with centrifugal loads are described in V.H. Lysiak & M.Y. Olinyk (2021), which establishes the dependence of thermal processes on the hydrodynamic parameters of the flow. The results showed that changes in hydrodynamic conditions directly affect the intensity of electric drive heating, which is characteristic of pumping stations where the load is formed precisely by the dynamics of the liquid medium. At the level of microdynamics of structures, the study by I. Biliuk *et al*. (2023) analysed the influence of the accuracy of movement control on the vibration loads transmitted to the insulation nodes and determining their structural stability. The analysis found that even minor fluctuations can cause accelerated accumulation of microdefects in the material. For systematic load control, I.I. Yaremak & V.S. Kostyshyn (2020) proposed an approach in which the optimisation of the operating modes of electromechanical complexes reduces the amplitude of peak impacts and stabilises the operational condition of the insulation.

Despite a wide range of works, scientific discourse has considered only certain aspects of the action of electrical, thermal, or mechanical factors; at the same time, their integrated action in the conditions of agro-industrial electric drives has not been sufficiently studied. In particular, there is a lack of comprehensive studies that reconcile the effects of partial discharges, thermal cycling, starting pulses, and microvibrations in the context of nanocomposite materials. This necessitates experimental and numerical analysis aimed at determining the patterns of degradation and assessing the impact of design and material modifications. In this regard, the aim of the study was to establish the patterns of behaviour of polymer and nanocomposite insulation of high-voltage circuit breakers in dynamic modes of operation of electric drives to assess the impact of electrical, thermal and mechanical loads, as well as the role of frequency converters and structural characteristics of composites on the durability of insulation.

The aim of the study was to establish the patterns of degradation of polymer and nanocomposite insulation of high-voltage circuit breakers under the action of electrical, thermal and mechanical loads characteristic of the dynamic operating modes of agro-industrial electric drives. To achieve this aim, three objectives were set: to establish the patterns of degradation of the electrophysical parameters of insulation under the action of dynamic electrothermal and mechanical modes; to evaluate the influence of silicon dioxide (SiO_2) and hexagonal boron nitride (h-BN) on the stability of electrical strength, thermal profile and nature of microstructural defects; to determine the effectiveness of frequency converters in reducing starting and thermal loads and in increasing the service life of high-voltage insulation in agro-industrial electric drives.

MATERIALS AND METHODS

The study was conducted between March and October 2025 in laboratory and production conditions, which ensured accurate reproduction of the electromechanical loads characteristic of high-voltage vacuum circuit breaker operation. The study included three material systems: unfilled epoxy resin (EP), a composite with dispersed silicon dioxide (NP), and a composite with hexagonal boron nitride (NC). The dispersed particles of SiO_2 and h-BN had a diameter of 80-120 nm and a mass fraction of 8%. The samples were prepared by casting followed by thermal stabilisation at 130°C and vacuum drying for 72 hours in a Memmert GmbH drying oven (Memmert GmbH, Germany). Material constants, in particular relative dielectric permeability (εr), thermal conductivity (λ) and density (ρ) for EP (epoxy polymer), NP (nanofilled polymer) and NC (nanocomposite), were determined based on laboratory measurements and used as input parameters for finite element method (FEM) models. Electrostatic and thermal modelling of insulation nodes was performed using ANSYS Maxwell and ANSYS Icepak software environments (ANSYS Inc., USA) based on three-dimensional (3D) geometric models of VD4 series vacuum circuit breaker insulators (ABB/Hitachi Energy).

The study was conducted in five interrelated stages. At the first stage of the study, the basic electrical and thermal characteristics of materials were determined in accordance with ASTM standards, in particular dielectric strength (ASTM D149-20, 2020), electrical resistance and conductivity of insulation (ASTM D257-14, 2021), thermal diffusion (ASTM E1461-13, 2022) and sample preparation conditions (ASTM D618-21, 021), which ensured the formation of reliable initial parameters for further numerical modelling and comparative analysis. The electrophysical characteristics of the insulation were measured in accordance with IEC 60270:2025 (2025) on a high-voltage test rig from Haefely Test AG (Switzerland), recording partial discharges, their onset and extinction voltages, time-frequency spectra of pulses and their evolution after

various numbers of load cycles. Phase-resolved partial discharge (PRPD) analysis was performed in accordance with the recommendations of IEC 60270:2025 for the classification of discharge types and the determination of the phase reference of pulses. The breakdown strength was determined by the method of increasing sinusoidal voltage with a gradient of 2 kV/s.

At the next stage of the study, switching overvoltages and transient recovery voltage (TRV) parameters were evaluated. The relevant parameters were determined in accordance with the requirements of the IEC 62271-100:2021 (2021) series of standards by reproducing the pulse modes characteristic of vacuum circuit breakers in systems with frequent electric drive starts. Controlled pulses were generated on a Haefely Test AG device with front and duration fixed in accordance with the standardised TRV zones. The parameters obtained were used to model the field strength and thermal peaks in the insulation nodes. In the third stage of the study, the influence of dynamic operating modes was evaluated by loading insulation samples with 1,000 starting cycles, which made it possible to simulate the cumulative effect of impulse electrothermal loads characteristic of the operation of electric drives in pumping, ventilation and grain drying systems. The starting processes were reproduced on an ABB M3AA electric motor (ABB Group, Italy) with a power of 7.5 kW in direct-on-line starting mode and in a configuration with a Danfoss VLT FC302 frequency converter (Danfoss A/S, Denmark).

The fourth stage of the study involved thermographic analysis and verification of thermal models of insulation nodes by assessing the impact of the frequency converter on electrical and thermal loads. To do this, direct-on-line (DOL) and frequency-controlled drive start-up modes were compared, recording start-up currents, PD parameters in accordance with IEC 60270:2025, and the spatial-temporal temperature distribution according to data from a FLIR T660 thermal imager. The starting currents were recorded with Chauvin Arnoux current clamps (Chauvin Arnoux, France) with a time resolution of 1 ms, and the temperature fields were monitored with a FLIR T660 thermal imager (FLIR Systems Inc., USA) with a temperature sensitivity of 0.03°C. Based on the obtained thermograms, spatial maps of thermal fields in static and dynamic modes were formed after a specified number of starting cycles, which made it possible to identify areas of local overheating, evaluate their geometry, and track the evolution of thermally stressed areas during the loading process. To quantitatively assess the impact of different start-up scenarios, the maximum temperature deviations (ΔT) obtained from thermographic measurements and thermal modelling in ANSYS Icepak were compared for DOL and frequency converter start-up modes. This ensured the verification of thermal models and allowed the assessment of the effectiveness of frequency control in terms of reducing thermal loads on insulation components.

In the fifth stage of the study, accelerated ageing, microstructural and reliability analysis methods were applied to comprehensively assess the degradation processes and service life of insulation materials. Accelerated operational ageing was implemented by thermal cycling in the range of 25-95°C with alternating heating and cooling phases, while the samples were additionally subjected to mechanical microvibration on a TIRA TV 51144 vibration stand (TIRA GmbH, Germany) with an amplitude of 0.4-0.7 mm in the frequency range of 10-80 Hz. Microstructural changes were recorded using a JEOL JSM-IT200 scanning electron microscope (JEOL Ltd., Japan), which enabled analysis of cracks, interphase defects and adhesion failures. Tracking resistance was determined in accordance with IEC 60587:2007 (2007) on an ELLAB TRK6 (ELLAB Group, Italy) installation, and dielectric spectroscopy was performed on a Novocontrol Alpha-A (Novocontrol Technologies, 2020, Germany) analyser. The service life of insulation materials was evaluated using Weibull curves in the ReliaSoft Weibull++ v9 software environment (ReliaSoft Corporation, USA). Statistical processing of experimental data was performed in OriginPro 2024 (OriginLab Corporation, USA) using Student's t-test, Mann-Whitney U-test and 95% confidence intervals at a significance level of $p < 0.05$. Economic calculations were performed using the total cost of ownership (TCO) model, which took into account the cost of materials, replacement frequency, emergency downtime, and the impact of frequency control on extending equipment life. The assessment was performed for a fixed six-month operating interval, which corresponded to approximately 180-220 start-up cycles in typical operating modes of pumping stations and grain drying complexes and included maintenance costs, replacement of degraded insulation components, and losses associated with equipment downtime. A further assessment of the five-year operating cycle was carried out by extrapolating the 6-month TCO values obtained.

RESULTS

The influence of dynamic electrical modes on changes in the electrophysical parameters of insulation

A comparative analysis of experimental results revealed differences in the values of specific resistance and breakdown voltage between the studied material systems after exposure to pulsed electrical modes. The data obtained reflected the unequal

response of EP, NP and NC materials to identical electrical influences, which made it expedient to compare them in a post-loading state. The differences identified were systematic in nature and could be traced in several electrophysical indicators. The set of measured parameters formed individual electrophysical profiles for each material, suitable for quantitative intermaterial comparison. The generalised results of measurements of specific resistance and breakdown voltage before and after electrical loading are given in Table 1. The data presented was used as an initial empirical array for further analysis of changes in the electrophysical characteristics of materials in the post-loading state.

Table 1. *Breakdown voltage and specific resistance indicators before and after exposure to impulse modes (EP, NP, NC)*

Material type	Specific resistance before (Ohm·m)	Specific resistance after (Ohm·m)	Breakdown voltage before (kV)	Breakdown voltage after (kV)
EP	1.2×10^{13}	6.3×10^{12}	18.7	13.9
NP (SiO_2)	3.5×10^{13}	2.9×10^{13}	22.5	20.3
NC (BN)	4.1×10^{13}	3.8×10^{13}	24.1	22.4

Source: *compiled by the authors based on ASTM D149-20 (2020), ASTM D257-14 (2021), IEC 60270:2025 (2025)*

According to Table 1, all materials studied showed a decrease in electrophysical characteristics after loading compared to the initial values. At the same time, the scale of these changes differed significantly between materials, which made it possible to identify clear differences in the nature of the transformation of their electrophysical properties. EP epoxy resin experienced the greatest decrease in electrophysical characteristics after impulse loading: its specific resistance decreased by 47.5% and its breakdown voltage by 25.7%. These changes were accompanied by an increase in the intensity of partial discharges, recorded in accordance with the registration criteria of the IEC 60270:2025 (2025) standard, which reflected the formation of local microchannels of increased electrical conductivity and a gradual weakening of the dielectric barrier in the polymer matrix. For the NP (nanocomposite with silicon dioxide), the amplitude of changes was more moderate: the specific resistance decreased by 17%, and the breakdown voltage by 9.8%. The highest stability was demonstrated by the NC (nanocomposite with hexagonal boron nitride), where the decrease in these parameters was 7.3% and 7.1%, respectively. The difference in the magnitude of deviations between EP, NP and NC reflected the material-dependent nature of degradation processes – from the maximum sensitivity of unfilled resin to the increased stability of nanocomposites due to the influence of the filler on the interphase structure and charge localisation mechanisms. Despite the recorded changes, for all materials studied, the breakdown voltage after loading remained within the ranges defined by baseline measurements in accordance with ASTM D149-20 (2020), and the specific volume resistance values did not exceed the functionally acceptable limits regulated by ASTM D257-14 (2021). Control tests after 1,000 cycles showed no signs of progressive or avalanche-like degradation: the values of electrical strength and specific resistance stabilised and did not show further decline. This indicated that even with increased PD activity, the post-load transformation of the electrophysical properties was local and non-cumulative.

A comparative analysis showed that EP was characterised by the greatest amplitude of changes, while NP and NC nanocomposites were noted for their increased resistance to impulse modes due to the stabilising effect of interphase regions and the barrier role of the nanofiller. The increase in PD activity was common to all the materials studied, but its scale depended on the composition of the composite: the introduction of SiO_2 or BN fillers led to a decrease in the density of local defect regions, which manifested itself in less pronounced changes in the parameters of partial discharges. The results obtained quantitatively reflected material-dependent differences in the change in specific resistance, breakdown voltage, and partial discharge intensity for EP, NP, and NC in the post-loading state. For nano-filled systems, the deviation values were lower compared to epoxy resin, which was confirmed by the recorded parameters. The presented data outlined the quantitative relationships between the studied material systems and reflected the peculiarities of their behaviour under post-loading conditions.

Results of modelling electrostatic and electrothermal fields in switch nodes

Numerical 3D-FEM modelling of electrostatic and electrothermal fields in the insulation nodes of a high-voltage switch allowed to identify characteristic spatial features of the distribution of electric field strength and temperature. Local maxima of both quantities were formed mainly in areas with variable curvature geometry and contrasting dielectric properties of materials. In the basic EP configuration, increased electric field values were observed at the inner radii of the ribs, at the polymer-metal

transitions, and in areas of local changes in the geometric profile. Parametric variations in geometry, in particular changes in the radius of curvature, channel depth, and the presence of internal cavities, led to a redistribution of the vector field and a shift in the areas of local maxima.

To clearly demonstrate the spatial differences in the distribution of electric field strength and temperature among the three configurations studied, comparative maps of the electric and thermal fields were provided (Fig. 1).

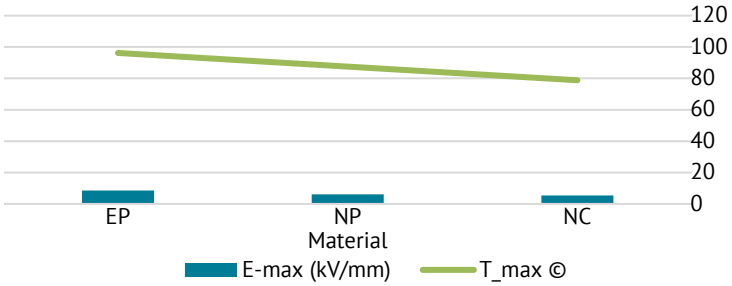

Figure 1. *Maximum values of electric field strength and temperature for EP, NP and NC materials*
Source: *compiled by the authors based on ASTM D149-20 (2020), ASTM D257-14 (2021), IEC 60270:2025 (2025)*

As shown in Figure 1, the maximum electrical and thermal parameters varied sequentially depending on the material configuration of the node. For the base material EP, the highest peak values of electric field strength and temperature were recorded, reaching approximately 8.6 kV/mm and 96.2°C, respectively. The lowest values of both parameters were observed for the NC configuration, where the maximum electric field strength did not exceed 5.4 kV/mm, and the temperature was about 78.8°C, indicating a more uniform electro-thermal distribution in this system under the simulation conditions. Such a coordinated change in electrical and thermal indicators indicated the existence of a relationship between the concentration of the electric field and local heat generation in the switch nodes. Quantitatively, this manifested itself in a gradual decrease in the maximum values of the electric field strength and the corresponding peak temperatures in the direction from EP to NC. The generalised quantitative values of the peak electrothermal parameters for all configurations are given in Table 2.

Table 2. *Maximum E-field and temperature values at key points of the nodes (three types of geometry)*

Configuration	E-field, max (kV/mm)	Temperature, max (°C)
EP (basic)	8.6	96.2
NP (SiO_2)	6.1	87.5
NC (BN)	5.4	78.8

Source: *compiled by the authors based on IEC 62271-100:2021 (2021), IEC 60270:2025 (2025)*

Analysis of Table 2 showed a consistent relationship between node configuration and electrical and thermal load levels. The values of 5.4 kV/mm stress and 78.8°C temperature obtained for the NC configuration indicated the influence of internal screens and the BN layer on the redistribution of the electric field and the formation of heat-conducting zones. The transition from EP to NP and NC was accompanied by a decrease in maximum electrical and temperature indicators, which was consistent with changes in geometry and material composition. The NP configuration demonstrated the effect of the SiO_2 nanofiller on field distribution equalisation and heat dissipation improvement compared to EP, while NC was characterised by lower integral parameters due to a combination of material and design factors. A comparison of these options demonstrated the existing relationship between the internal structure, the properties of the materials used, and the behaviour of the node under combined electrical and thermal loads. The obtained dependence indicates the need to consider several material and design parameters when designing high-voltage insulation components operating in variable electromechanical modes.

Thermographic analysis of damage and overheating areas

The thermographic results obtained after 1,000 start-up cycles under electrothermal load conditions reflected the spatial distribution of temperature along the surface of the insulation assembly in the post-load state and characterised its integral thermal behaviour. Temperature fields were recorded along the entire

length of the unit surface, which made it possible to record temperature variations within a single coordinate axis. The thermographic images obtained made it possible to assess the integral thermal state of the insulation structure after cyclic loading and to identify characteristic areas with elevated temperatures. To summarise the results and provide a comparative analysis, the temperature distribution was presented as a linear temperature profile, which allowed for a comparison of the thermal behaviour of different material configurations within a single coordinate system. A graphical representation of the temperature distribution along the surface of the insulation unit after 1,000 start-up cycles is shown in Figure 2.

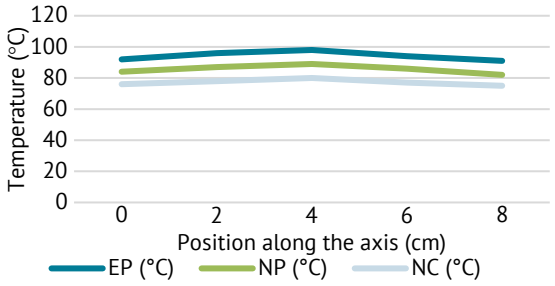

Figure 2. *Temperature distribution graph along the surface of the insulation unit after 1,000 cycles*
Source: *compiled by the authors*

According to the data shown in Figure 2, after completing 1,000 start-up cycles for all studied material configurations, a clearly pronounced temperature maximum was recorded in the central part of the insulation node, located at a distance of approximately 4 cm from the initial coordinate. In the edge zones of the surface, the temperature values systematically decreased, resulting in the formation of a stable dome-shaped temperature distribution profile along the axis, characteristic of the post-load quasi-stationary thermal state of the insulation structure. The overall configuration of the temperature profiles was similar for EP, NP and NC materials, indicating the reproducibility of the spatial structure of the thermal field at a constant node geometry regardless of the material composition of the insulation. At the same time, the absolute temperature levels showed clear intermaterial differences. For EP epoxy resin, the maximum recorded temperature reached about 98°C, for NP nanocomposite – about 89°C, while for the NC configuration it did not exceed 80°C. Throughout the entire range of coordinates studied, the temperature values for EP remained higher than those for nano-filled systems, which was clearly visible in the linear temperature profiles. The minimum temperature values along the surface of the insulation node were also material-dependent and amounted to about 90-91°C for EP, 82-83°C for NP, and 74-75°C for NC.

Accordingly, the temperature difference along the node axis was approximately 7°C for EP, about 6°C for NP, and about 5°C for NC, which quantitatively reflected different levels of thermal unevenness under the same geometric conditions and load regime. Analysis of the shape of the temperature profiles revealed the presence of local temperature increases along the surface of the insulation node, the spatial position of which was similar for all material configurations. At the same time, the amplitude of these local maxima significantly depended on the material: the largest deviations were observed for EP, smaller ones for NP, while for NC they were minimal. This led to different degrees of temperature heterogeneity of the insulation surface after cyclic electrothermal loading. A comparative analysis of temperature profiles showed that with a decrease in maximum temperatures in nano-filled systems, the temperature gradient along the surface of the insulation node also decreased. EP was characterised by the largest temperature difference, NP by a moderate one, while NC by a minimal one.

The results obtained made it possible to quantitatively characterise the level of temperature heterogeneity for each material configuration in the post-loading state and to use these parameters for further comparison with the electrophysical indicators of insulation. The spatial consistency of the experimentally recorded temperature maxima with the results of electrothermal modelling confirmed the reproducibility of the formed temperature profiles and their stability after multi-cycle loading. In general, the thermographic results quantitatively reflected the material-dependent differences in the thermal regime of insulation nodes for EP, NP and NC after 1,000 start-up cycles. For EP epoxy resin, the highest peak temperatures and the greatest unevenness of the temperature field were recorded, while for nano-filled systems NP and NC, a consistent decrease in maximum temperatures and smoothing of temperature gradients along the surface of the insulation node was observed, indicating a more stable thermal behaviour of these materials in the post-loading state.

The effect of frequency converters on insulation loads

A comparative analysis of DOL starting and starting using a Danfoss VLT FC302 frequency converter revealed fundamental differences in the nature of the electromechanical and electrothermal load on the insulation nodes of high-voltage circuit breakers. The use of a frequency converter led to the transformation of the starting process from a short-term pulse mode to a controlled quasi-stationary mode with a gradual increase

in voltage and current, which significantly affected the distribution of the electric field and current loads in polymer and nanocomposite insulation. This change in the starting mode resulted not only in a decrease in the peak amplitudes of the electrical parameters, but also in a modification of the time structure of the transition process, determining a different nature of the action of electrical and electromechanical loads on the insulating elements in the initial phase of operation and reducing the intensity of extreme influences critical for the degradation mechanisms of the material. Under direct-on-line start-up conditions, peak instantaneous currents in the range of 5.3-5.8 I_n were recorded, accompanied by increased levels of electrostatic stresses in the interphase regions of insulating materials and local inhomogeneities of the electric field. Such conditions corresponded to an increase in the electrothermal load on the insulation nodes, which manifested itself in an increase in temperature, the formation of temperature gradients, and an increase in the intensity of partial discharges in the first start-up cycles. Starting via a frequency converter was characterised by a smoothed load profile due to a gradual increase in voltage and current: the starting current amplitude decreased to 1.9-2.3 I_n, while there was a decrease in switching overvoltages and temperature peaks in the initial stage of equipment operation. A quantitative assessment showed that the average starting current in DOL mode was about 5.6 I_n, while when using a frequency converter, its value was in the range of 1.9-2.3 I_n throughout the entire transition process.

The reduction in current loading was accompanied by a decrease in transient recovery voltage (TRV) amplitude and the voltage rise rate (dV/dt), which are key characteristics of electrical stress acting on insulation assemblies during start-up. The combination of the recorded changes reflects the differences in electromechanical start-up conditions for the two scenarios and their impact on insulation element loading. The comparative parameters of the starting modes for direct-on-line starting and starting using a variable frequency drive (VFD) are summarised in Table 3.

Table 3. *Parameters of high-voltage electric drive starting modes for DOL and VFD starts*

Parameter	DOL	VFD (Danfoss VLT FC302)
Average starting current, I_p/I_n	5.6	2.1
Amplitude of switching transient recovery voltage (TRV), kV	2.8-3.4	1.1-1.4
Voltage rise rate dV/dt, kV/μs	0.95-1.20	0.18-0.25
Output voltage waveform	Pure sinusoidal waveform, voltage step at energisation	Pulse-width modulation (PWM) modulation with high-frequency pulses, smooth voltage ramp-up
Start-up duration, s	0.35-0.45	1.8-2.4
Duration of current above 3 I_n, ms	160-190	18-25
Peak insulation temperature during the first 10 cycles, °C	92-98	71-78

Source: *compiled by the authors based on IEC 62271-100:2021 (2021)*

Analysis of the data presented in Table 3 showed that the use of a frequency converter significantly changed the electromechanical start-up profile of the high-voltage electric drive. The highest starting current values were observed in direct starting mode and reached about 5.6 I_n, while when using a frequency converter, they decreased to a level not exceeding 2.1 I_n. This reflected a significant reduction in the impulse current load in the regulated start mode. A similar trend was observed for switching overvoltages. In DOL mode, the maximum TRV values reached approximately 3.4 kV, while during start-up via a frequency converter, they decreased to a level of about 1.1 kV. At the same time, the voltage rise rate in direct start mode reached values of about 1.2 kV/μs, while in regulated mode it decreased to about 0.2 kV/μs. This indicated a significant mitigation of electrical transient processes when using frequency control. Analysis of the time characteristics of the start showed that direct start was implemented as a short-term but sharply pulsed mode, while start using a frequency converter was characterised by a longer duration and reduced peak values of electrical parameters. Particularly indicative was the reduction in the time the current remained at levels exceeding 3 I_n: from approximately 190 ms in DOL mode to about 20 ms in regulated start mode. These changes were accompanied by a decrease in peak insulation temperatures recorded in the initial phase of equipment operation. The results of thermographic measurements were consistent with the differences in electrical modes and confirmed the formation of different types of electrical and thermal loads on insulation nodes during direct and controlled starts. According to the data obtained, the peak insulation temperatures in the first start-up cycles when using a frequency converter were 18-22°C lower compared to the direct start mode. For an

integrated assessment of the accumulated thermal load, a comparison of temperature increments Δ*T* for both start-up scenarios was made, the results of which are presented in Figure 3.

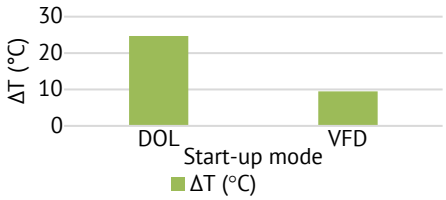

Figure 3. *Comparison of thermal load on insulation (ΔT) for two start-up modes*
Source: *compiled by the authors*

The data shown in Figure 3 demonstrated significant differences in the accumulated thermal load of insulation nodes for two electric drive start-up scenarios, caused by the different nature of transient electrical modes. In DOL mode, the maximum average thermal overload exceeded the baseline by 24.7°C, reflecting the intense pulsed nature of the electrothermal impact on insulation materials in the initial operating cycles and the formation of localised overheating zones. In contrast, when using a frequency converter, the temperature increase decreased to 9.5°C, which indicated a limitation of peak thermal loads due to the controlled increase in current and voltage and a more uniform distribution of heat flows in the insulation elements. Thus, the regulated start-up resulted in a 61.5% reduction in the temperature increase Δ*T*, which reflected a decrease in the electrothermal load on the polymer and nanocomposite insulation in the starting modes. The decrease in the amplitude Δ*T* when operating with a frequency converter was consistent with the parameters of electrical processes recorded during starting tests. Lower values of starting currents, switching overvoltage amplitudes and voltage rise rates dV/dt led to a reduction in electrical losses and local heat generation in the interphase areas of insulation materials. As a result, a thermal regime with less pronounced temperature peaks compared to the direct start-up mode was formed in the insulation nodes. The results obtained showed that the use of a frequency converter changed the thermal response of the insulation nodes from impulsive to stabilised with lower values of integral temperature overload. The recorded quantitative differences reflected the influence of the starting mode on the electrothermal state of the insulation and the role of the controlled electromechanical load in the formation of the thermal operating conditions of high-voltage circuit breakers.

Mechanical degradation of insulation and microstructural analysis of materials

During accelerated tests simulating the actual operating conditions of high-voltage circuit breakers in pumping stations and grain drying installations, typical manifestations of surface degradation of polymer and nanocomposite insulation were recorded, caused by the combined action of operational factors. The formation of degradation damage occurred under the influence of thermal fluctuations, PD activity, mechanical vibrations, as well as impulse starting modes characteristic of the operation of electric drives of agro-industrial equipment under variable loads. These factors created an uneven electrothermal and mechanical impact on the insulation materials, which contributed to the initiation and development of surface defects. Microstructural analysis of the sample surfaces, performed using scanning electron microscopy (SEM, JEOL JSM-IT200), revealed fundamental differences in the mechanisms and morphology of damage for the three material systems studied: EP (unfilled epoxy matrix), NP (nano-filled polymer) with SiO_2 particles, and composite structure with a NC (boron nitride shielding layer). EP was characterised by the presence of developed track formations with carbonised edges, accompanied by a branched network of microcracks, indicating intensive surface degradation. The NP material, in turn, showed a significantly lower density of damage, which manifested itself in the form of limited local micropores and isolated linear defects without the formation of continuous track channels. In the NC configuration, only isolated submicron damage was recorded, localised mainly in the near-surface zone at the boundary between the BN layer and the polymer matrix, with no signs of through-track or defect coalescence into extended degradation structures. The quantitative distribution of the frequency of defects is shown in Figure 4.

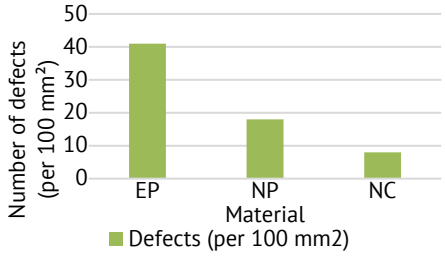

Figure 4. *Frequency of detection of microstructural defects after thermal and vibration tests*
Source: *compiled by the authors*

The data shown in Figure 4 showed that the epoxy system (EP) was characterised by the highest frequency of surface microdefects, exceeding

40 pores and cracks per 100 mm^2, which indicated the intensive development of degradation processes under combined electrothermal and mechanical loading. The recorded damage density for EP was approximately 2.3 times higher than the corresponding values for the SiO_2 nanocomposite (NP) and more than five times higher than for the NC (BN-shielded configuration). This quantitative distribution was consistent with differences in degradation mechanisms, confirmed by SEM observations. EP was characterised by the formation of deep track channels with carbonised edges and developed secondary microcracks, which contributed to further concentration of the electric field and acceleration of surface destruction. The NP material showed limited areas of defects, which were mainly represented by isolated micropores and linear surface cracks without the formation of continuous track structures. The smallest number of localised damages in the NC system was due to the action of the BN shielding layer, which contributed to the equalisation of local electrical and thermal stresses, reduction of electric field gradients at the interphase boundary, and suppression of the initiation and development of through tracking. For an additional assessment of the resistance of materials to surface degradation, tracking resistance tests were carried out, the results of which are presented in Table 4.

Table 4. *Tracking resistance of insulating materials under standard loading conditions*

Configuration	Time to breakdown, min	Nature of damage	Comparative Tracking Index (CTI) class
EP (basic)	9.3	Deep carbonised tracks	IIb (100-175 V)
NP (SiO_2)	21.8	Localised surface tracking marks	IIa (175-250 V)
NC (BN+ shielding layer)	>30 (no breakdown)	Absence of continuous tracking	I (≥250 V)

Source: *compiled by the authors based on IEC 60587:2007 (2007)*

A comparison of the values in Table 4 demonstrated fundamental differences between the three material systems. The EP material was characterised by the shortest time to breakdown (≈9.3 min), accompanied by the formation of deep carbonised tracks. The NP material showed an increase in the time to breakdown and the appearance of only surface traces, indicating increased tracking resistance due to the modification of the interphase region with SiO_2 particles. The NC configuration demonstrated the highest tracking resistance: no conductive channel formation was observed during the test, and the material was classified as CTI Class I – the level required for high-voltage systems with increased surface reliability requirements. The results obtained indicated the presence of significant material-dependent differences in the nature of microstructural degradation and tracking resistance of the studied insulation systems under combined operational loads. The EP was characterised by the highest frequency of surface microdefects, intensive development of secondary microcracking and the formation of deep carbonised tracks under the action of thermal, electrical and mechanical factors. The SiO_2 nanocomposite showed a reduction in the number and length of defects, as well as an increase in the time to breakdown compared to EP, indicating the effect of stabilisation of the interphase region and slowing down of degradation processes. The configuration with a BN shielding layer was characterised by the lowest density of localised damage and the absence of through-tracking within the standard tests according to IEC 60587:2007 (2007), confirming the high surface stability of this system. The recorded quantitative differences reflected the specifics of degradation mechanisms for the three material systems and determined their behaviour under typical operating loads of agro-industrial electrical complexes.

Resource assessment and parameter dispersion (Weibull analysis)

The Weibull analysis method was used to quantitatively assess the durability of insulating materials and the statistical dispersion of failure parameters during cyclic testing. This approach made it possible to describe the probabilistic nature of failures and establish the relationship between the accumulated cyclic load and the frequency of breakdowns. The initial data for the analysis were the experimentally recorded values of the number of cycles to failure for each sample of EP, NP and NC insulating materials. Based on these data, statistical processing was performed to construct generalised probability curves for each material system. The resulting curves reflected the change in the probability of failure depending on the level of accumulated cyclic load. The constructed Weibull curves allowed for a comparative assessment of the resource and the nature of the distribution of failures between the materials under study. The generalised results of the analysis in the form of model Weibull curves are shown in Figure 5.

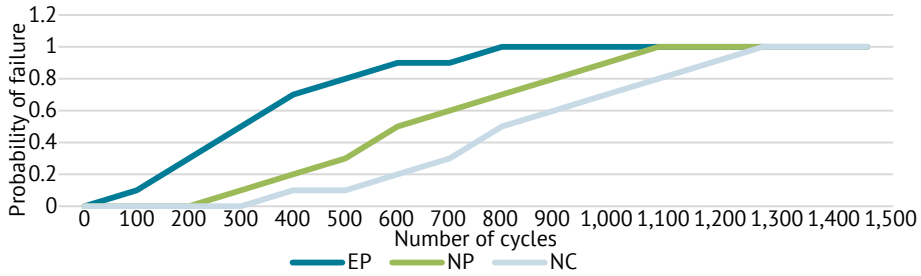

Figure 5. *Weibull curves for insulation materials based on cyclic test results*
Source: *compiled by the authors*

As shown in Figure 5, the EP epoxy material demonstrated the highest probability of failure across the entire range of cyclic loading studied, which was reflected in the sharply rising shape of the Weibull curve compared to the NP and NC nanomodified systems. Already in the early cycle range, approximately 300-400, the failure probability for EP reached values of about 0.5, indicating a significant proportion of early failures and a limited initial life of the material. In the range of average operating hours, approximately 800-900 cycles, the EP curve practically approached the level of 0.95-1.0, which corresponded to almost complete failure in the studied sample. The nano-filled polymer NP was characterised by a flatter Weibull curve trajectory and its systematic shift towards higher resource values. In the early cycle zone, the failure probability for NP did not exceed approximately 0.15, while in the range of 800-900 cycles it was about 0.8, which indicated a more uniform distribution of operating time to failure and a reduced proportion of premature failures compared to epoxy resin EP. The lowest failure probability values were recorded for the NC nanocomposite throughout the entire cyclic loading range studied. In the range of 300-400 cycles, it did not exceed about 0.05, and in the range of 800-900 cycles, it reached only 0.55-0.6, which reflected a significant shift in the resource of this material towards higher values of cyclic fatigue. A clear gap between the EP, NP and NC curves indicated a systemic difference in the nature of damage accumulation and failure realisation for different material configurations. A generalised analysis of representative sections of the Weibull curves confirmed that the epoxy material EP was characterised by the highest proportion of early failures, the nano-filled polymer NP occupied an intermediate position in terms of reliability, while the nanocomposite NC demonstrated the lowest probability of failure at the same levels of cyclic loading. The quantitative results of the evaluation of the Weibull parameters β and η for the three types of materials are given in Table 5, which made it possible to formalise the identified differences in terms of statistical reliability.

Table 5. *Shape (β) and scale (η) parameters of dispersion for three types of insulation*

Material type	β (shape coefficient)	η (average service life, hours)
EP (epoxy)	1.52	380
NP (SiO_2)	2.63	715
NC (BN)	3.41	912

Note: *the value of the scale parameter η was obtained by converting the number of cycles to failure into time resources under steady-state operation with a fixed start frequency; data for a temperature of 95°C was obtained within a separate thermally loaded series*
Source: *compiled by the authors*

The data in Table 5 showed significant differences in the resource characteristics of the three insulation configurations studied under cyclic thermoelectric loading conditions. For the EP epoxy system, the average resource was about 380 hours, which corresponded to the lowest durability among the materials studied. For the NP nano-filled polymer, an increase in the average resource to 715 hours was recorded, while for the NC nanocomposite, the resource reached 912 hours. Compared to EP, the resource of NP increased by approximately 1.9 times, and the resource of NC by 2.4 times, which indicated a fundamentally different nature of degradation processes in these material systems. Analysis of the Weibull distribution parameters showed that the EP epoxy configuration was characterised by the lowest values of the β shape parameter, which corresponded to a significant statistical dispersion of the resource and the presence of an early

failure zone. This behaviour indicated the dominance of local defects and uneven degradation development in the polymer matrix. For the NP configuration, the β value increased, reflecting a decrease in the variability of the time to failure and a more stable nature of degradation processes. The highest β values were recorded for the NC nanocomposite, which corresponded to the most compact distribution of the resource and the absence of a pronounced early failure zone. The results of tests at an elevated ambient temperature (95°C) showed a decrease in the scale parameter η for all configurations studied, but the intensity of this decrease varied significantly. For EP, the value of η decreased to 290 hours, indicating the high sensitivity of the material to thermoelectric loads. For NC, the η parameter remained at a level not lower than 840 hours, confirming the significantly higher thermal stability and resource stability of nanocomposite insulation. The NP configuration occupied an intermediate position between EP and NC, demonstrating moderate resource degradation at elevated temperatures. A comparative analysis showed that the NC configuration combined the highest values of the β and η parameters among all the materials studied, which corresponded to the maximum resource and minimum variability of the time to failure. The NP configuration was characterised by intermediate resource indicators, while EP demonstrated the lowest resource and the greatest statistical dispersion. The results obtained allowed to conclude that the durability and stability of insulation materials were determined by microstructural homogeneity and the effectiveness of interphase interaction. The NC configuration demonstrated the highest β and η values, indicating low resource variability and high safety margin, making it most suitable for use in high-voltage switches for agricultural and industrial applications.

Resistance of insulating materials to partial discharges under load

The PD data obtained showed differences in the behaviour of the three insulation systems under the influence of cyclic electromechanical loading. For EP epoxy insulation, after 500 cycles, a sequential increase in the amplitude and frequency of pulses was recorded, indicating the formation of local microdefects and areas of increased electrical stress. At the 1,000-cycle stage, the amplitudes of partial discharges in EP reached the maximum values among the materials studied, and the recorded pulses were characterised by an ordered phase structure and an extended amplitude range, reflecting the development of intense electrophysical processes in the material. In the NP nanocomposite with SiO_2 inclusions, the increase in discharge activity was recorded at significantly later stages of loading and had a lower intensity. The pulses showed lower peak values, occurred irregularly, and were recorded mainly at the end of the cycles. This dynamic indicated a more uniform distribution of the electric field and a slower development of localised defects in the material without the formation of stable discharge activity channels. The NC composite with a BN layer and internal shielding showed the lowest level of partial discharges throughout the test period. The pulses were at the background noise level or below the detection threshold, and after 1,000 cycles, no pulse grouping or amplitude jumps were recorded. This behaviour corresponded to the increased structural stability of the material, in which the BN layer and shielding elements ensured the equalisation of the electric field and reduced sensitivity to accumulated defects. The differences found between the materials reflected different mechanisms of their microstructural stability and ability to counteract localised electrical processes under cyclic loading. Typical PD oscillograms of the three materials after 1,000 cycles are shown in Figure 6.

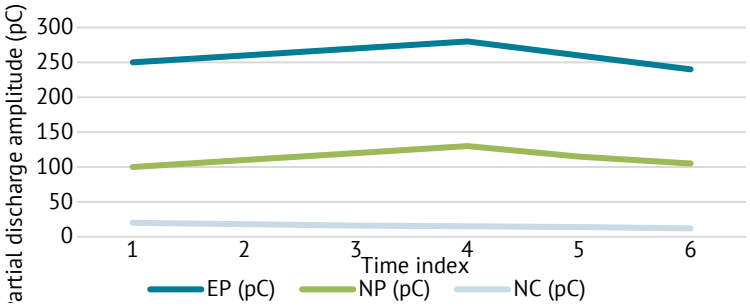

Figure 6. *Pulse activity of partial discharges in various insulating materials (after 1,000 cycles)*
Source: *compiled by the authors based on IEC 60270:2025 (2025)*

According to the results of Figure 6, for EP, the maximum pulse amplitude reached 280 pC at a frequency of about 35 pulses/s. This intensity corresponded to the presence of structural inhomogeneities, micropores,

and interphase disturbances. In NP, the amplitude did not exceed 145 pC, and the pulses were single in nature. For NC, the amplitudes of partial discharges were in most cases below the registration threshold, which confirmed the high homogeneity of the dielectric structure and the effective operation of internal shielding elements. A comparison of the experimental data with the results of modelling in ANSYS Maxwell confirmed that in EP, the maximum electric fields were concentrated at the joints of the edges and local cavities. It was these geometric features that contributed to the initiation of partial discharges. In NC, internal shielding equalised the stress at critical points, reducing the probability of breakdown and the formation of discharge channels. This explained the lower amplitude of partial discharges and the absence of significant defects even after 1,000 cycles. To quantitatively assess PD resistance, the initiation voltage (PDIV) and extinction voltage (PDEV) were determined. The results are shown in Table 6.

Table 6. *Electrical parameters of partial discharges after 1,000 cycles*

Configuration	PDIV, kV	PDEV, kV	voltage hysteresis (Δ*U*), kV
EP (basic)	3.6	2.4	1.2
NP (SiO_2)	4.7	3.8	0.9
NC (BN+ shielding layer)	5.5	5.0	0.5

Source: *compiled by the authors based on IEC 60270:2025 (2025)*

As shown in Table 6, the NC configuration demonstrated the highest resistance to partial discharges, with a PDIV of 5.5 kV, which was 53% higher than that of EP. The hysteresis value Δ*U* for NC was 0.5 kV, the lowest among all the investigated materials, reflecting only a minor change in breakdown voltage under cyclic loading. The NP configuration incorporating SiO_2 exhibited intermediate PDIV and Δ*U* values, indicating partial electric field equalisation and enhanced thermal stability of the matrix compared with EP. Analysis of the PRPD distributions showed that surface partial discharges with pronounced phase correlation predominated in EP and NP, whereas in NC most pulses remained at background level or below the detection threshold, without signs of clustering or amplitude surges. The phase-resolved pulse distribution in NC was characterised by low PD intensity across all investigated cycles, while EP and NP exhibited peak activity within specific phase intervals. The combination of high PDIV values, low hysteresis Δ*U*, and minimal pulse activity demonstrated that the NC composite with a BN layer and internal shielding maintained stable electrophysical parameters after 1,000 loading cycles. These characteristics support the applicability of NC in high-voltage circuit breakers operating under variable and high-stress conditions in pumping stations and grain-drying complexes, ensuring more uniform electric field distribution and reducing the likelihood of local defects and the development of breakdown channels.

The economic feasibility of introducing new materials and frequency converters

To provide a generalised and systematic presentation of the obtained experimental results, a comparative assessment was performed on the technical and economic indicators of high-voltage insulation units operated within the electric drives of pumping stations and grain drying complexes under cyclic loading conditions. The analysis incorporated PD parameters, specifically the PDIV, Δ*U*, average amplitude-frequency characteristics of partial discharges, and the proportion of samples exhibiting microstructural damage. In addition to electrophysical indicators, economic parameters were included in the comparison, represented as the TCO over a fixed operating period. These indicators characterised insulation units with different material configurations under identical operating conditions, allowing for a comparison of their technical state and economic costs during the initial stage of operation. The summarised values of the relevant parameters following a six-month cyclic load are presented in Table 7.

Table 7. *Technical and economic performance of high-voltage insulation units under a 6-month cyclic loading period*

Material configuration	PDIV, kV	Δ*U*, kV	Proportion of samples with damage, %	Average PD amplitude, mV	Average PD repetition rate, pulses/min	TCO over 6 months, USD
EP (without VFD)	3.6	1.5	28	220	45	280
NP (without VFD)	4.8	1.0	12	160	30	140
NC (without VFD)	5.5	0.5	3	80	12	50
EP + VFD	3.6	1.5	28	220	45	150

Table 7, Continued

Material configuration	PDIV, kV	Δ*U*, kV	Proportion of samples with damage, %	Average PD amplitude, mV	Average PD repetition rate, pulses/min	TCO over 6 months, USD
NP + VFD	4.8	1.0	12	160	30	70
NC + VFD	5.5	0.5	3	80	12	50

Note: *economic indicators are given in USD per high-voltage insulation unit*
Source: *compiled by the authors*

Analysis of the data in Table 7 showed that the insulation materials studied differed significantly in terms of their combined electrophysical characteristics and total operating costs during the first six months of cyclic operation. Within the interpretation of the results obtained, the five-year operating period corresponded to a total load equivalent to approximately 18,000-22,000 electric motor starts in variable operating modes, taking into account scheduled technical inspections, routine downtime and unscheduled shutdowns associated with insulation degradation and component failures. EP epoxy insulation was characterised by the lowest partial discharge initiation voltage values and the highest operating costs among all configurations considered. Already during a six-month period of operation, EP showed significant voltage hysteresis (ΔU = 1.5 kV) and the formation of microstructural damage in 28% of samples. The increased values of the average partial discharge amplitude (220 mV) and frequency (45 pulses/min) correlated with the development of surface and interphase defects characteristic of the electrical ageing processes of the polymer matrix. The combination of these factors resulted in total cost of ownership of USD 280 over a six-month period, which, when extrapolated to a five-year operating cycle, corresponded to USD 620-780 per insulation unit, taking into account several replacements and losses associated with emergency equipment downtime. For nano-filled polymer NP with SiO_2 filler, other quantitative ratios of electrophysical and economic parameters were established. An increase in the partial discharge initiation voltage to 4.8 kV and a decrease in the voltage hysteresis to 1.0 kV were accompanied by a decrease in the proportion of damaged samples to 12%. The average values of the amplitude and frequency of partial discharges (160 mV and 30 pulses/min, respectively) indicated a less intense degradation process compared to epoxy insulation. This was directly reflected in the economic indicators: the TCO for six months was USD 140, and the projected costs for a five-year operating cycle were in the range of USD 280-350. The most favourable technical and economic characteristics were demonstrated by the NC nanocomposite with a BN layer and internal shielding. The partial discharge initiation voltage reached 5.5 kV with a minimum voltage hysteresis (Δ*U* = 0.5 kV), accompanied by low partial discharge intensity: the average amplitude did not exceed 80 mV, and the frequency was about 12 pulses/min. The proportion of samples with microstructural damage did not exceed 3%, which was consistent with the uniform distribution of the electric field and limited development of degradation processes. Under these conditions, the TCO for a six-month period was USD 50, and the cost for a five-year operating cycle was estimated at USD 90-120 without the need for scheduled replacement of the insulation unit. A comparative analysis of configurations using frequency converters showed that their use did not change the established electrophysical parameters of insulating materials, but significantly affected economic indicators by reducing the number of hard start-up modes, reducing the amplitude of short-term overvoltages, and reducing the frequency of emergency and unscheduled equipment shutdowns. Within the scope of the analysis, the total cost of ownership was formed by the costs of scheduled and unscheduled maintenance, replacement of degraded components, and losses associated with downtime, while maintaining clear differences between EP, NP, and NC materials throughout the entire life cycle of operation

DISCUSSION

The results of electrical, thermal and mechanical measurements showed that polymer dielectrics demonstrate different sensitivity to dynamic load modes, and the behaviour of nanocomposite systems is determined by the ability of their interphase structure to compensate for local peaks of stress and temperature. A 25-30% reduction in the breakdown voltage of epoxy insulation after cyclic electrothermal loading and a corresponding decrease in specific volume resistance correlate with the "moisture-heat-defect" model described by J. Ma *et al.* (2023), which established that hygrothermal effects cause hydrolytic destruction of the ester bonds of the epoxy matrix, degradation of interphase areas, and accumulation of microdefects, which determine the accelerated deterioration of electrophysical characteristics and a reduction in the service life of the insulation material. The difference in structural stability between

the epoxy system and nanocomposites confirms the mechanisms described by F. Wiesbrock (2014), which emphasised that nanofillers form a modified interphase zone with increased resistance to the concentration of electrical and mechanical stresses. The decrease in the amplitude of the breakdown voltage drop in materials with SiO_2 and BN is consistent with the author's approach, which links the stability of electrophysical parameters with the damping of local overvoltages in a nanostructured environment. This correlation provided a basis for further analysis of the behaviour of nanocomposites in more complex modes with a combination of partial discharges, thermomechanical loads and high-frequency voltage components.

The increase in the intensity of degradation processes in polymer insulation under the action of repeated impulse influences correlates with the conclusions of M. Ghassemi (2019), which stated that fast voltage fronts and repeated high-frequency pulses create conditions for accelerated electrothermal destruction. The similarity lies in the observation of a pattern: the greatest deterioration in parameters occurs in systems without nanomodification, where there are no mechanisms for dissipating electrical peaks. The scenarios of insulation depletion under the action of fast pulses described by the author are consistent with the observed difference between EP, NP and NC in terms of breakdown voltage, specific resistance and partial discharge activity. The presence of thermal anomalies in areas of sharp geometric changes and at polymer-metal boundaries is consistent with the trends identified by M. Hu *et al*. (2022), where it is emphasised that local thermal maxima are an early marker of interphase destruction and gas evolution. The recorded temperature peaks in the joint areas and in the insulation ribs demonstrate the same pattern: areas of reduced thermal conductivity and field concentration become centres of thermochemical destruction. The coordination of the identified mechanisms confirmed the importance of thermographic monitoring in high-voltage systems. The formation of localised areas of elevated temperature in the polymer matrix is consistent with the results of O. Sakhno *et al*. (2025), which showed that online diagnostics of high-voltage equipment under operating voltage allows the detection of thermal anomalies caused by the concentration of electrical and thermal stresses in insulation nodes. The authors noted that the spatial distribution of temperature can serve as an indicator of areas of potential electrical instability, which, during prolonged operation, transform into centres of partial discharge activation. In the study, these provisions were extended to the level of materials science, which was confirmed by the analysis of thermographic profiles of polymer and nanocomposite samples and their correlation with the quantitative parameters of partial discharges.

The observed increase in the intensity of partial discharges under the action of cyclic electrothermal loading demonstrates a clear dependence on the frequency and shape of the pulses, which is consistent with the conclusions of Q. Li *et al*. (2015). The authors showed that high-frequency components accelerate the formation of microcavities and increase the intensity of PD activity already in the early stages of ageing, which is consistent with the increased sensitivity of unmodified polymer systems to initiation processes. The tendency of epoxy resin to sharply decrease the "non-discharge stability" interval completely repeats the patterns described in high-frequency modes of electrothermal ageing. The spatial displacement of defect zones towards areas with an uneven electric field and reduced heat dissipation properties is consistent with the results of Y. Wu *et al*. (2022), where it was proven that the combination of geometric inhomogeneities and local thermal maxima increases the probability of degradation channel formation. The mechanism described by the authors – "geometric field concentration → local overheating → microcrack → gas-filled cavity" – fully explains the fixed trend of increased partial discharge activity in joint and edge areas. The mechanisms presented in the study are consistent with the interpretation of the shift of the maximum discharge area as a consequence of interphase instability. The identified relationship between the frequency of trigger pulses, the amplitude of PD activity, and geometric features repeats the results of D. Verginadis *et al*. (2021), where it is noted that a combination of electrical and structural factors determines the specific discharge energy and degradation rate. The authors showed that even moderate pulses in the presence of a heterogeneous polymer structure form accelerated destruction scenarios, which is consistent with the observed changes in the structure of EP samples. The refined model of action shows that the combination of solid surface defects with impulse loading creates a stable mechanism for the development of discharge erosion, which determines the specific discharge energy and the rate of material degradation. The peculiarities of the effect of distorted voltage on the acceleration of electrical ageing correspond to the patterns described by D. Fabiani & G.C. Montanari (2001). The authors demonstrated that harmonic components and voltage distortions significantly increase the rate of destruction of polymer insulation due to the nonlinear amplification of electrical stresses in interphase zones. The detected changes in the frequency spectrum of discharge activity are

consistent with the authors' statement regarding the critical role of high-frequency components as factors determining the resource stability of insulation.

The synergistic action of amplitude and frequency distortions explains the accelerated deterioration of the parameters of epoxy samples. The reduction in stress gradients and thermal peaks in nanocomposite structures is consistent with the trends described by L. Lusuardi *et al*. (2019), where it was proven that systems optimised for operation with inverter drives have improved resistance to dynamic modes. The authors emphasised that the correct choice of material can significantly reduce the level of partial discharges in systems with PWM voltage, which is consistent with the observed difference between EP and NC in the intensity of discharge activity after 1,000 start-up cycles. The mechanism is based on the ability of nanocomposites to smooth out local electrical peaks, which in traditional materials become triggers for early breakdown. The increased stability of electrical strength and reduced variability (Weibull β) in NP and NC samples is consistent with the concept of nanodielectrics presented by W. Liu *et al*. (2018). The work emphasised that nanoparticles form a modified interphase region with optimised polarisation, which increases the material's resistance to stress and discharge erosion. The observed increase in the β parameter is consistent with the authors' statement regarding the increase in structural homogeneity and the reduction in the number of defective channels, which in polymer systems without nanomodification remain one of the main sources of degradation.

The further increase in resistance to cyclic loading in BN samples correlates with the conclusions of T. Tanaka (2025), which presents a modern interpretation of the "two-layer interphase structure" mechanism that provides improved dielectric permeability and stability during repeated temperature fluctuations. The increase in breakdown voltage and reduction in losses are consistent with the author's model, which explains that nanoparticles with high thermal conductivity are capable of reducing local temperature peaks, which are the main factor in the thermoelectric degradation of polymers. The enhancement of dielectric properties in BN-modified samples and their reduced sensitivity to impulse loads are consistent with the results of A. Alsoud *et al*. (2025). The authors showed that rare earth oxide nanoparticles form stable heat dissipation channels, which significantly reduces local overheating and accelerated ageing. The obtained Weibull coefficients β and η are consistent with the concept that thermally stable nanofillers act as barriers to microcrack development. The identified patterns of changes in the thermal profile and PD activity in frequent start-up modes are consistent with the review by A.A. Razi-Kazemi & K. Niayesh (2021), which emphasised that the most dangerous scenarios for switching equipment are precisely dynamic modes with repeated pulses. The authors noted that the combination of electrical peaks and vibration loads forms accelerated degradation trajectories, which explains the faster reduction in the service life of traditional polymers. The dynamic nature of the load, caused by the peculiarities of hydraulic processes in pumping systems, is consistent with the conclusions of V.S. Kostyshyn & I.I. Yaremak (2017), where it is proven that optimising modes can significantly reduce peak electromechanical effects. The observed reduction in thermal instability when working with frequency converters repeats the trends described by the authors, who emphasised the ability of optimised control to reduce the amplitude of transient processes. The energy effect of using frequency drives and the reduction in costs associated with insulation degradation are consistent with the results of L. Elmahni *et al*. (2021), which proved that frequency control in pumping systems provides a significant reduction in heat generation and an increase in overall efficiency. The similarity is explained by the mechanism of reducing starting currents and stabilising the operating point of the unit. The assessment of the economic feasibility of using new materials and frequency control is consistent with the approach of N. Dutta *et al*. (2023), who demonstrated that digital life cycle analysis methods can reveal hidden operating costs. The reduction in costs over the long term confirms the authors' key conclusion about the dependence of system durability on the nature of load modes. The identified effectiveness of resource and economic solutions correlates with the conclusions of K. Zhang *et al*. (2026), who noted the importance of combining technical and environmental and economic criteria when selecting energy technologies. The reduction in operating cycle costs and the increase in energy efficiency are consistent with the patterns described by the authors.

The systematised results show that the combination of nanomodified insulation structures and regulated start-up modes forms a coordinated circuit of electrothermal processes, in which the amplitude of partial discharges, thermal gradients and the number of microstructural defects are reduced. Such dependencies correlate with established experimental models of nanodielectrics, where interphase layers determine the distribution of field intensity and local heat dissipation parameters. The observed increase in the β parameter in the Weibull curves is consistent with the mechanisms of resource stabilisation of composites with highly thermally conductive fillers described in the

world literature. The reduction in starting current load when using frequency regulation corresponds to the technical and operational patterns according to which a decrease in impulse electrical and thermal effects leads to a reduction in the rate of defect accumulation in polymer dielectrics. The set of comparisons collected demonstrates the formation of a structurally consistent picture of degradation processes, reflecting key trends in research on high-voltage insulation and systems with electromechanical cycles of increased dynamics.

CONCLUSIONS

The study allowed for a comprehensive characterisation of the degradation and reliability of polymer and nanocomposite insulating materials of high-voltage vacuum circuit breakers in dynamic operating modes of electric drives of pumping stations and grain drying complexes. It has been established that the combination of impulse starting loads, cyclic thermal effects and mechanical vibrations creates critical operating conditions in which the ability of the material to limit localised electrophysical and microstructural degradation processes is decisive. It has been shown that an epoxy matrix without fillers is characterised by the highest sensitivity to dynamic modes. After cyclic loading, the specific resistance decreased by more than 47%, the breakdown voltage by more than 25%, and the activity of partial discharges was accompanied by the formation of tracking structures and a significant loss of resource. Nanofilling with silicon dioxide provides a moderate improvement in performance: the specific resistance decreased by about 17%, and the breakdown voltage by 9.8%, while the development of partial discharges was limited and unstable without the formation of stable discharge channels. The highest stability was demonstrated by the configuration with hexagonal boron nitride and internal shielding, for which the reduction in specific resistance and breakdown voltage did not exceed 7.1-7.3%, the partial discharge initiation voltage reached 5.5 kV, and no through-tracking was formed in standard tests. Numerical 3D-FEM modelling combined with thermography showed a consistent decrease in peak electric field strength from 8.6 kV/mm for EP to 5.4 kV/mm for NC, and maximum temperatures from approximately 96°C to 79°C after 1,000 start-up cycles. Weibull analysis confirmed significant differences in durability: the average life of epoxy insulation was about 380 hours, while for nanocomposites it increased to 700-900 hours with a simultaneous decrease in statistical dispersion. It was found that the use of frequency converters reduces starting currents from about 5.6 I_n to 2.1 I_n and reduces the integral temperature increase of the insulation by 61.5%, forming a stabilised thermal regime. A technical and economic analysis showed that the TCO over a six-month period decreases from about 280 USD for epoxy insulation to about 50 USD for BN-containing configurations, with a multiple reduction in projected costs over a five-year operating cycle.

The results obtained indicate the promise of integrating composites with highly thermally conductive fillers and frequency control to optimise the operation of agro-industrial systems, in particular pumping stations, fan modules, grain drying units and greenhouse installations. Further research should focus on analysing the behaviour of composites in ultra-long cycles, modelling degradation under stochastic loads, expanding the range of nanofillers, and developing predictive models for digital technical diagnostic systems.

ACKNOWLEDGEMENTS

None.

FUNDING

None.

CONFLICT OF INTEREST

None.

REFERENCES

[1] Alsoud, A., Shaheen, A.A., Tofel, P., Knápek, A., & Sobola, D. (2025). Enhancing dielectric properties of epoxy-based nanocomposites reinforced with yttrium oxide (Y_2O_3) nanoparticles for high-voltage insulation applications. *Materials Science and Engineering: B*, 320, article number 118407. doi: 10.1016/j.mseb.2025.118407.

[2] ASTM D149-20. (2020). *Standard test method for dielectric breakdown voltage and dielectric strength of solid electrical insulating materials at commercial power frequencies*. Retrieved from https://standards.iteh.ai/catalog/standards/astm/5415b498-6eb9-4a94-84fa-bb451ebefae3/astm-d149-20?srsltid=AfmBOoolVOLhGZ_0rzlp2i-ySWzCpf7oALMFHVB4F53jbX3FvI9ItW5c.

[3] ASTM D257-14. (2014). *Standard test methods for DC resistance or conductance of insulating materials*. Retrieved from https://www.astm.org/d0257-14.html.

[4] ASTM D618-21. (2021). *Standard practice for conditioning plastics for testing*. Retrieved from https://surl.li/ccmyth.

[5] ASTM E1461-13. (2022). *Standard test method for thermal diffusivity by the laser flash method*. Retrieved from https://store.astm.org/e1461-13r22.html.

[6] Biliuk, I., Shareyko, D., Savchenko, O., Havrylov, S., Mardziavko, V., & Fomenko, L. (2023). Tracking system of a micromanipulator based on a piezoelectric motor. In *2023 IEEE 5th international conference on modern electrical and energy system*. Kremenchuk: IEEE. doi: 10.1109/MEES61502.2023.10402375.
[7] Dutta, N., Palanisamy, K., Shanmugam, P., Subramaniam, U., & Selvam, S. (2023). Life cycle cost analysis of pumping system through machine learning and hidden Markov model. *Processes*, 11(7), article number 2157. doi: 10.3390/pr11072157.
[8] Elmahni, L., Assalaou, K., Aitiaz, E., Benachir, B., & Bouhouch, L. (2021). Technico-economic study of a photovoltaic pumping system using a variable-frequency drive converter. *E3S Web of Conferences*, 229, article number 01017. doi: 10.1051/e3sconf/202122901017.
[9] Fabiani, D., & Montanari, G.C. (2001). The effect of voltage distortion on ageing acceleration of insulation systems under partial discharge activity. *IEEE Electrical Insulation Magazine*, 17(3), 24-33. doi: 10.1109/57.925300.
[10] Ghassemi, M. (2019). Accelerated insulation aging due to fast, repetitive voltages: A review identifying challenges and future research needs. *IEEE Transactions on Dielectrics and Electrical Insulation*, 26(5), 1558-1568. doi: 10.1109/TDEI.2019.008176.
[11] Hu, M., Tang, B., Liang, Q., Luo, Z., Luo, C., Wang, J., Zhang, L., & Zhu, L. (2022). Monitoring and prediction of thermal failure of high-voltage switchgear insulation materials by studying the thermodynamic properties of FR-4 epoxy resin and the characteristic gas of thermal decomposition. *Journal of Physics: Conference Series*, 2387, article number 012028. doi: 10.1088/1742-6596/2387/1/012028.
[12] IEC 60270:2025. (2025). *High-voltage test techniques – charge-based measurement of partial discharges*. Retrieved from https://webstore.iec.ch/en/publication/65087.
[13] IEC 60587:2007. (2007). *Electrical insulating materials used under severe ambient conditions – test methods for evaluating resistance to tracking and erosion*. Retrieved from https://webstore.iec.ch/en/publication/2526.
[14] IEC 62271-100:2021. (2021). *High-voltage switchgear and controlgear – part 100: Alternating-current circuit-breakers*. Retrieved from https://webstore.iec.ch/en/publication/62785.
[15] Iegorov, O.B., Kundenko, M.P., Iegorova, O.Yu., Mardziavko, V.A., & Rudenko, A.Yu. (2025). The influence of the design of the stator winding of a synchronous-reactive generator on increasing its energy efficiency. *Electrical Engineering & Electromechanics*, 5, 3-9. doi: 10.20998/2074-272X.2025.5.01.
[16] Kostin, O.M., Yaros, O., Yaros, Y., Savenko, A., Martynenko, V., & Boyko, I. (2022). Method for evaluating the stability of arc burning of electrodes with rutile-cellulosic covering. In *2022 IEEE 4th international conference on modern electrical and energy system*. Kremenchuk: IEEE. doi: 10.1109/MEES58014.2022.10005682.
[17] Kostyshyn, V.S., & Yaremak, I.I. (2017). Mathematical model of reliability and efficiency of pumping unit of an oil pumping station. *Scientific Bulletin of National Mining University*, 5, 62-68.
[18] Li, Q., Liu, W., Han, S., & Lu, X. (2015). Analysis of partial discharge characteristics of epoxy resin insulation during high-frequency electrothermal combined aging. *High Voltage Engineering*, 41(2), 389-395. doi: 10.13336/j.1003-6520.hve.2015.02.005.
[19] Liu, W., Cheng, L., & Li, S. (2018). Review of electrical properties for polypropylene based nanocomposite. *Composites Communications*, 10, 221-225. doi: 10.1016/j.coco.2018.10.007.
[20] Lusuardi, L., Cavallini, A., Gómez de la Calle, M., Martínez-Tarifa, J.M., & Robles, G. (2019). Insulation design of low voltage electrical motors fed by PWM inverters. *IEEE Electrical Insulation Magazine*, 35(3), 7-15. doi: 10.1109/MEI.2019.8689431.
[21] Lysiak, V.H., & Oliinyk, M.Y. (2021). Simulation of dynamic operating modes of asynchronous electric drive with centrifugal pump load. *Reporter of the Priazovskyi State Technical University. Section: Technical Sciences*, 42, 113-121. doi: 10.31498/2225-6733.42.2021.240665.
[22] Ma, J., Yang, Y., Wang, Q., Deng, Y., Yap, M., Chern, W.K., Oh, J.T., & Chen, Z. (2023). Degradation and lifetime prediction of epoxy composite insulation materials under high relative humidity. *Polymers*, 15(12), article number 2666. doi: 10.3390/polym15122666.
[23] Matvienko, M.V., Martynenko, V.O., & Vakhonina, L.V. (2023). Stress-strain state of joints with a soft interlayer under mechanical loading. *International Applied Mechanics*, 59, 100-106. doi: 10.1007/s10778-023-01203-3.
[24] Razi-Kazemi, A.A., & Niayesh, K. (2021). Condition monitoring of high voltage circuit breakers: Past to future. *IEEE Transactions on Power Delivery*, 36(2), 740-750. doi: 10.1109/TPWRD.2020.2991234.
[25] Sakhno, O., Skrupska, L., Odiyaka, K., Vasylevskyi, V., & Shylo, S. (2025). Diagnostics of the technical state of high-voltage equipment under operating voltage. *Technology Audit and Production Reserves*, 2(1(82)), 35-44. doi: 10.15587/2706-5448.2025.325777.

[26] Shcherba, A.A., Shcherba, M.A., & Peretyatko, Ju.V. (2023). Electro-physical processes of degradation of cross-linked polyethylene insulation of power cables and self-carrying insulated wires under non-sinusoidal voltages and currents. *Theoretical Electrical Engineering and Electrophysics*, 1, 3-6. doi: 10.15407/techned2023.01.003.
[27] Silnyk, M., & Fedynets, V. (2025). Application of thermal imaging diagnostics for technical maintenance of electrical centralization devices in railway automation systems. *Energy Engineering and Control Systems*, 11(1), 44-52. doi: 10.23939/jeecs2025.01.044.
[28] Stavinskii, A., & Koshkin, D. (2021). Technical solutions of laminated magnetic cores of transformers with combination of electrical steel. In *2021 IEEE international conference on modern electrical and energy systems*. Kremenchuk: IEEE. doi: 10.1109/MEES52427.2021.9598810.
[29] Stavinskiy, A., Tsyganov, A., Babenko, D., & Sadovoy, O. (2022). Comparison of thermal loads of a single-phase transformer with a laminated magnetic core. In *2022 IEEE 4th international conference on modern electrical and energy systems*. Kremenchuk: IEEE. doi: 10.1109/MEES58014.2022.10005642.
[30] Tanaka, T. (2025). Progress in nanodielectrics: Future from the past decade. *IEEE Transactions on Dielectrics and Electrical Insulation*, 32(1), 102-116. doi: 10.1109/TDEI.2024.3487813.
[31] Verginadis, D., Karlis, A., Danikas, M.G., & Antonino-Daviu, J.A. (2021). Investigation of factors affecting partial discharges on epoxy resin: Simulation, experiments, and reference on electrical machines. *Energies*, 14(20), article number 6621. doi: 10.3390/en14206621.
[32] Wiesbrock, F. (2014). *Nano- and microcomposites for electrical engineering applications*. Basel: MDPI. doi: 10.3390/books978-3-03842-293-8.
[33] Wu, Y., Ding, D., Wang, Y., Zhou, C., Lu, H., & Zhang, X. (2022). Defect recognition and condition assessment of epoxy insulators in gas insulated switchgear based on multi-information fusion. *Measurement*, 190, article number 110701. doi: 10.1016/j.measurement.2022.110701.
[34] Yaremak, I.I., & Kostyshyn, V.S. (2020). Control of modes of electrohydraulic complex on the basis of a system approach. *Scientific Bulletin of UNFU*, 30(3), 83-88. doi: 10.36930/40300314.
[35] Zhang, K., Mo, J., Liu, Z., Yin, W., Wu, F., & You, J. (2026). Life cycle environmental and economic impacts of various energy storage systems: Eco-efficiency analysis and potential for sustainable deployments. *Integrated Environmental Assessment and Management*, 22(1), 289-302. doi: 10.1093/inteam/vjaf035.
[36] Zidane, O., Haller, R., Trnka, P., & Bärnklau, H. (2025). Lifetime behavior of turn insulation in rotating machines under repetitive pulsed stress. *Energies*, 18(14), article number 3826. doi: 10.3390/en18143826.

Вплив динамічних режимів роботи електроприводів насосних станцій та зерносушильних комплексів на деградацію нанокомпозитної ізоляції високовольтних вимикачів: результати вимірювань і рекомендації для агроінженерії

Андрій Ставинський
Доктор технічних наук, професор
Миколаївський національний аграрний університет
54008, вул. Георгія Ґонґадзе, 9, м. Миколаїв, Україна
https://orcid.org/0000-0001-7573-9238
Лариса Вахоніна
Кандидат фізико-математичних наук, доцент
Миколаївський національний аграрний університет
54008, вул. Георгія Ґонґадзе, 9, м. Миколаїв, Україна
https://orcid.org/0000-0002-1668-2275
Володимир Мартиненко
Кандидат технічних наук, доцент
Миколаївський національний аграрний університет
54008, вул. Георгія Ґонґадзе, 9, м. Миколаїв, Україна
https://orcid.org/0000-0003-4067-3640
Віталій Мардзявко
Магістр, асистент
Миколаївський національний аграрний університет
54008, вул. Георгія Ґонґадзе, 9, м. Миколаїв, Україна
https://orcid.org/0000-0001-7327-9215
Андрій Руденко
Магістр, асистент
Миколаївський національний аграрний університет
54008, вул. Георгія Ґонґадзе, 9, м. Миколаїв, Україна
https://orcid.org/0000-0002-5103-6412

Анотація. Дослідження було спрямоване на визначення впливу електричних, теплових і механічних навантажень на довговічність полімерної та нанокомпозитної ізоляції високовольтних вимикачів, що застосовуються у насосних станціях і зерносушильних комплексах України. Методологія поєднувала чисельне моделювання електростатичних і теплових полів у тривимірних конструкціях ізоляційних вузлів, прискорені термоциклічні та механічні випробування, аналіз часткових розрядів за міжнародними стандартами, термографічний контроль, мікроструктурні дослідження та статистичну оцінку ресурсу на основі кривих надійності. Установлено, що традиційна епоксидна ізоляція зазнає найбільш інтенсивної деградації: після циклічних навантажень питомий опір зменшувався на 47,5 %, пробивна напруга – на 25,7 %, а середній ресурс становив близько 380 годин. Для нанонаповненого матеріалу з діоксидом кремнію зниження питомого опору обмежувалося 17 %, пробивної напруги – 9,8 %, при збільшенні середнього ресурсу до 715 годин. Найвищу стабільність продемонструвала ізоляція з гексагональним нітридом бору та внутрішнім екрануванням, для якої зміни електрофізичних параметрів не перевищували 7,3 % за питомим опором і 7,1 % за пробивною напругою, напруга початку часткових розрядів досягала 5,5 кВ, а середній ресурс становив близько 912 годин. Чисельні та експериментальні результати показали зниження пікової напруженості електричного поля з 8,6 до 5,4 кВ/мм і максимальних температур з 96,2 до 78,8°C після 1 000 пускових циклів. Застосування керованих пускових режимів дозволило зменшити пускові струми з 5,6 In до приблизно 2,1 In та знизити інтегральне теплове навантаження ізоляції на 61,5 %. Техніко-економічна оцінка засвідчила зменшення сумарної вартості володіння за шість місяців з 280 до 50 доларів США на один ізоляційний вузол, що підтверджує практичну доцільність впровадження нанокомпозитів і керованих режимів пуску в агропромислових електроприводах. Практична значущість отриманих результатів полягає у формуванні критеріїв для вибору матеріалів та режимів роботи електроприводів з метою підвищення надійності комутаційного обладнання в агропромислових електромеханічних системах та використання моделювальних і діагностичних підходів для прогнозування деградації й оптимізації конструкцій ізоляційних вузлів

Ключові слова: часткові розряди; епоксидна смола; електротеплове навантаження; діелектрична міцність; відновлювана напруга; частотне регулювання; мікроструктурні дефекти